THE ASTROPHYSICAL JOURNAL, 490:92–98, 1997 November 20


# CAN INTERNAL SHOCKS PRODUCE THE VARIABILITY IN GAMMA-RAY BURSTS?

SHIHO KOBAYASHI, TSVI PIRAN, AND RE'EM SARI
Racah Institute of Physics, Hebrew University, Jerusalem, 91904 Israel;
shiho@alf.fiz.huji.ac.il, tsvi@shemesh.fiz.huji.ac.il, sari@shemesh.fiz.huji.ac.il
*Received 1997 May 5; accepted 1997 June 30*

## ABSTRACT

We discuss the possibility that gamma-ray bursts result from internal shocks in ultrarelativistic matter. Using a simple model, we calculate the temporal structure and estimate the efficiency of this process. In this model the flow of ultrarelativistic matter is represented by a succession of shells with random values of the Lorentz factor. We calculate the shocks that take place between those shells, and we estimate the resulting emission. Internal shocks can produce the highly variable temporal structure observed in most of the bursts, provided that the source emitting the relativistic flow is highly variable. The observed peaks are in almost one-to-one correlation with the activity of the emitting source. A large fraction of the kinetic energy is converted to radiation. The most efficient case is when an inner engine produces shells with comparable energy but very different Lorentz factors. It also gives the most desirable temporal structure.

*Subject headings:* gamma rays: bursts — relativity — shock waves

## 1. INTRODUCTION

The Burst and Transient Source Experiment (BATSE) on the *Compton Gamma Ray Observatory* (*CGRO*) has revolutionized our ideas about the location of gamma-ray bursts (GRBs). The isotropy of the events and the paucity of weak bursts strongly support the cosmological origin of GRBs (Meegan et al. 1992; Paczyński 1992; Piran 1992; Nemiroff et al. 1994). The most fascinating mechanisms for producing cosmological GRBs are decelerations of ultrarelativistic matter having a Lorentz factor $\gamma \geq 100$. This provides the only known solution to the compactness problem (Piran 1996). The kinetic energy of the ultrarelativistic matter is converted into internal energy by relativistic shocks. These shocks can be due to the interstellar medium (ISM) ("external shocks") or shocks inside the shell itself due to nonuniform velocity ("internal shocks"). Electrons are heated by the shocks, and the internal energy is then radiated via synchrotron emission and inverse Compton scattering. Although the ultrarelativistic matter flow was originally considered in the dynamical context of a fireball (Shemi & Piran 1990; Paczyński 1990), one can imagine GRB models in which the fireball is replaced by some unknown nonthermal acceleration mechanism but the radiation still originates from slowing down of the ultrarelativistic matter (Piran 1996).

Most bursts have a highly variable temporal profile with a timescale of variability $\delta T$ significantly shorter than the overall duration $T$. A typical value is $\delta T/T \sim 10^{-2}$. Clearly any GRB model must be able to explain this complex temporal structure.

The naive "external shocks" scenario requires only one uniform shell. The complex structure is due to surrounding matter (ISM in some models and starlight in others; Shaviv & Dar 1995). Two of us have shown that the efficiency of this process is less than 1% (Sari & Piran 1997a). Using the observed variability scale $\delta T$, one can estimate the typical size of a single emitter. The number of emitters must be less than the number of peaks. The total area of all emitters is therefore only $\sim 1\%$ of the shell's area. Even a modified version of this model, in which the shell is composed of many smaller shells that collide one after the other with the ISM, is impossible. Most of the collisions would occur at a radius that satisfies $R \geq \Delta\gamma^2$, where $\Delta$ is the total width of the shells.[1] At this radius, angular spreading (Katz 1994; Fenimore, Madras, & Nayakshin 1996) will cause each peak to be spread on a timescale of $R/\gamma^2 c = \Delta/c$, which is also the total duration of the bursts. The observed bursts will therefore be smooth. The only way out, in the context of the external shock model, is for the shell to be replaced by a narrow and highly variable beam. However, the angular width of this beam must be less than $\delta T/(T\gamma) \approx 10^{-4}$!

The obvious alternative is the "internal shock" scenario (Rees & Mészáros 1994; Narayan, Paczyński, & Piran 1992). These shocks could occur within a variable relativistic wind produced by a highly variable source. Internal shocks do not suffer from the angular spreading problem. A fast shell that was injected after a slower one will eventually catch up and collide with it. If both shells have Lorentz factors of order $\gamma$, the time until collisions will be of order $\gamma^2 L/c$, where $L$ is the initial separation between the shells. The collision will therefore occur at radius $R = \gamma^2 L$, and the angular spreading time is of order of $L/c$. Since the total duration is given by the total width of the shells $\Delta/c \gg L/c$, the observed peak width is considerably smaller than the total width, and complex temporal structure is possible. In view of the difficulties within the external shock scenario, it is worthwhile to consider the question whether internal shocks could actually produce the temporal structure observed in GRBs and what the efficiency of this process would be.

To examine the energy conversion in internal shock, we construct, following Mochkovitch, Maitia, & Marques (1995), a simple model in which the ultrarelativistic wind is represented by many shells having a random distribution of intrinsic parameters. We calculate the energy conversion due to shocks that form between the shells, considering at each time a binary (two-shell) encounter. We show that internal shocks can produce the observed highly variable temporal profiles. We reproduce the result of Mochkovitch

[1] Distances, time, velocities $\beta$, and the corresponding Lorentz factors $\gamma$, are measured in the observer's rest frame. Thermodynamic quantities are measured in the fluid rest frame.

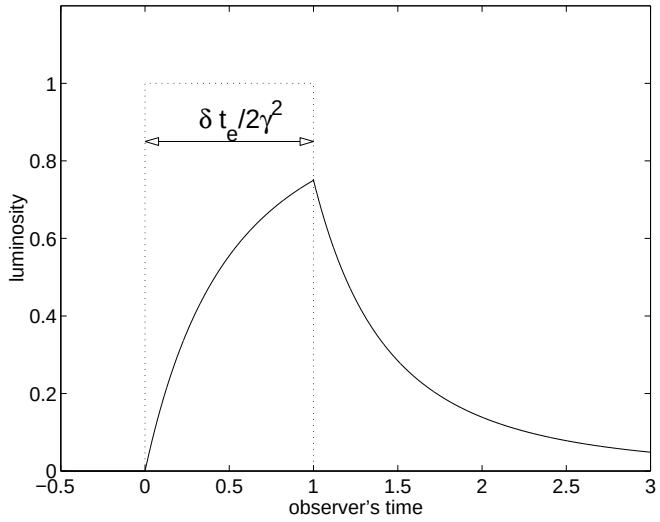


FIG. 1.—Peak produced by a collision between two shells: luminosity vs. observer's time. The solid line corresponds to $R = c\,\delta t_e$, and the dotted line corresponds to $R = 0$.

et al. (1995), who concluded that the efficiency of this process is low (<10%) if the spread in Lorentz factors is small. However, we show that higher efficiency could be achieved if the spread in the Lorentz factors of the ultrarelativistic matter is larger.

We explore in § 2 the basic unit of our model, the interaction of two shells. We explain in § 3 the algorithm for evolution of multiple shells. In §§ 4 and 5 we discuss the temporal structure and the efficiency, respectively. Finally we discuss the implications for observation in § 6.

## 2. TWO-SHELL INTERACTION

Internal shocks arise in a relativistic wind with a nonuniform Lorentz factor and convert a portion of the kinetic energy to radiation. We represent the irregular wind by a succession of relativistic shells. A collision of two shells is the elementary process in our model.

A rapid shell (denoted by the subscript $r$) catches up a slower one ($s$), and the two merge to form a single one ($m$). The system behaves like an inelastic collision between two masses $m_r$ and $m_s$. Using conservation of energy and momentum, we calculate the Lorentz factor of the merged shell to be

$$\gamma_m \simeq \sqrt{\frac{m_r\gamma_r + m_s\gamma_s}{m_r/\gamma_r + m_s/\gamma_s}}\,, \tag{1}$$

where $\gamma_i (\gg 1)$ and $m_i$ are the Lorentz factors and the masses of these shells. The internal energy of the merged shell is the difference of kinetic energy before and after the collision:

$$E_{\rm int} = m_r c^2(\gamma_r - \gamma_m) + m_s c^2(\gamma_s - \gamma_m)\,. \tag{2}$$

The efficiency of conversion of the kinetic energy into the internal energy in a single collision is given by

$$\epsilon = 1 - (m_r + m_s)\gamma_m/(m_r\gamma_r + m_s\gamma_s)\,. \tag{3}$$

The emitted radiation will be observed as a pulse with a width $\delta T$. Three timescales, the cooling time, the hydrodynamic time, and the angular spreading time, determine $\delta T$. [2] The internal energy is radiated via synchrotron emission and inverse Compton scattering. In most cases, the cooling timescale of electrons is much shorter than the hydrodynamic timescale (Sari, Narayan, & Piran 1996; Sari & Piran 1997b), so we can neglect the cooling time.

The hydrodynamic timescale is the time the shock crosses the shell. In fact there are two shocks, as the interaction between the two shells takes place in the form of two shocks: a forward shock and a reverse shock. Using conservation of mass, energy, and momentum at the shocks and equality of pressures and velocities along the contact discontinuity, one can derive the Lorentz factors of the forward and the reverse shocks $\gamma_{\rm fs}, \gamma_{\rm rs}$ (Sari & Piran 1995):

$$\gamma_{\rm fs} \simeq \gamma_m\sqrt{\left(1 + \frac{2\gamma_m}{\gamma_s}\right)\Big/\left(2 + \frac{\gamma_m}{\gamma_s}\right)}\,,$$
$$\gamma_{\rm rs} \simeq \gamma_m\sqrt{\left(1 + \frac{2\gamma_m}{\gamma_r}\right)\Big/\left(2 + \frac{\gamma_m}{\gamma_r}\right)}\,. \tag{4}$$

For simplicity, we estimate the emission timescale by the time at which the reverse shock crosses the rapid shell:

$$\delta t_e = l_r/c(\beta_r - \beta_{\rm rs})\,, \tag{5}$$

where $l_r$ is the width of the rapid shell. The emitting region moves toward the observer, and the observed timescale is shorter by a factor of $1/2\gamma_m^2$. If both shells have a Lorentz factor of order $\gamma$, this observed timescale is of order $l_r/c$.

If the collision of the shells takes place at a large radius $R$, angular spreading affects the width of the pulse. The separation of the shells is $L$, and the effect of angular spreading on the pulse width is $\sim L/c$, as we mentioned in § 1. If the separation $L$ is larger than the width of the shells $l$, the pulse width $\delta T$ is determined by angular spreading. The shape of the pulse becomes asymmetric with a fast rise and a slower decline (Fig. 1), which GRBs typically show. The peak amplitude is given by $E_{\rm int}\,c/l$. If angular spreading is significant, the amplitude is lower by a factor of $1 - (1 + l/L)^{-2}$. The observed luminosity, $\mathcal{L}$, is given by

$$\mathcal{L}(t) = \begin{cases} 0 & (t < 0)\,, \\ h[1 - 1/(1 + 2\gamma_m^2\,ct/R)^2] & (0 < t < \delta t_e/2\gamma_m^2)\,, \\ h\{1/[1 + (2\gamma_m^2\,t - \delta t_e)c/R]^2 - 1/(1 + 2\gamma_m^2\,ct/R)^2\} & \\ & (t > \delta t_e/2\gamma_m^2)\,, \end{cases} \tag{6}$$

where $h = E_{\rm int}\,2\gamma_m^2/\delta t_e$.

We assume that the internal energy produced by the collision is radiated isotropically in the shell's rest frame. We also assume that all the internal energy is radiated rapidly. In this case we obtain at the end of the collision a single cold shell whose Lorentz factor is $\gamma_m$, given by equation (1). The shocks compress the initial shells, and this results in a thinner shell with a width $l_m$:

$$l_m = l_s\,\frac{\beta_{\rm fs} - \beta_m}{\beta_{\rm fs} - \beta_s} + l_r\,\frac{\beta_m - \beta_{\rm rs}}{\beta_r - \beta_{\rm rs}}\,. \tag{7}$$

[2] Clearly, if the source is located at a high redshift $z$, all the observed timescales are stretched by a factor $1 + z$. However, as we are interested mainly in the ratio between the width of the peaks and the overall duration and in the efficiency energy conversion, this factor is unimportant.

The density is discontinuous through the contact discontinuity. For simplicity we average the density:

$$\rho_m = \frac{\rho_r l_r \gamma_r + \rho_s l_s \gamma_s}{l_m \gamma_m} . \quad (8)$$

We describe the resulting shell as a homogeneous shell with a constant density $\rho_m$ and a Lorentz factor $\gamma_m$.

While the shells propagate, their density decreases because of the spherical geometry. However, the density ratio between any two shells remains constant and the process depends just on the density ratio and not on the absolute value of the density. We expect, therefore, that this one-dimensional model captures the basic features of realistic events.

## 3. THE MULTIPLE-SHELL MODEL

We represent the irregular wind by a succession of relativistic shells with a random distribution of Lorentz factors and densities. A collision between two shells produces shocks that convert some of the kinetic energy of the shells to thermal energy. The thermal energy is then radiated via synchrotron emission and inverse Compton scattering. In § 2 we calculated the observed radiation produced by a collision between two shells. For multiple shells, numerous collisions take place. Each collision produces a pulse similar to that shown in Figure 1. To construct the temporal structure in a given model, we calculate the time sequence of the two-shell collisions and superimpose the resulting pulses from each collision.

Consider a wind consisting of $N$ shells. We assign an index $i$ ($i = 1, N$) to each shell according to the order of the emission from the inner engine. Each shell is characterized by four variables: a Lorentz factor $\gamma_i$, a density $\rho_i$ (the shells are cold and therefore the pressure satisfies $p_i \equiv 0$) a width $l_i$, and the time $\tilde{t}_i$ when the shell was ejected from the source. We choose the origin of time such that the last shell—the $N$th shell—is emitted at $\tilde{t}_N = 0$. Clearly all other shells are emitted earlier, so the $\tilde{t}_i$ are negative for $i < N$. At $t = 0$ the shells are at the following "initial" positions (inner edge): $R_i = -\tilde{t}_i \beta_i c$. We denote the distance at this stage between shell $i$ and shell $i + 1$ by $L_i$: $L_i \equiv R_i - R_{i+1} - l_{i+1}$. The time $l_i/c$ corresponds to the period during which the "inner engine" has operated, while $L_i/c$ corresponds to the period during which the "inner engine" was quiet. The size of the inner engine should, of course, be smaller than $l$ to produce a shell with a width $l$.

We turn now to evaluate the evolution of this multiple-shell system. There will be numerous collisions between different shells. We denote by the index $j$ the $j$th collision, which takes place at a time $t_j$ and position $R_c(t_j)$. For simplicity we define a zeroth collision at the initial time $t_0 = 0$; this enables us to put the first collision on a par with the rest. Given the velocities of the shells $\beta_i$ and their separation $L_i$ at $t_{j-1}$ we calculate the collision time for all pairs $(i, i + 1)$ satisfying $\beta_{i+1} > \beta_i$:

$$\delta t_{i,i+1} \equiv L_i/c(\beta_{i+1} - \beta_i) . \quad (9)$$

We then find the minimal collision time among all the $\delta t_i$:

$$\delta t_j = \min (\delta t_{i,i+1}) . \quad (10)$$

Let $s$ and $s + 1$ be the indices of the shells for which this minimum takes place. The $j$th collision is between the $s$ and the $s + 1$ shells and takes place at the time

$$t_j = t_{j-1} + \delta t_j \quad (11)$$

and at the position

$$R_c(t_j) = R_{s+1}(t_j) = R_{s+1}(t_{j-1}) + c\beta_{s+1}\,\delta t_j . \quad (12)$$

An observer at $R_0$ away from the central source will begin to detect radiation from this collision at a time

$$t_{\mathrm{obs},s} = [R_0 - R_c(t_j)]/c + t_j . \quad (13)$$

Note that, for reasons that will be clear later, we give this observed time the index $s$ of the outer shell that participated in the collision. At the end of the computation we set the minimum of $t_{\mathrm{obs},\,s}$ to be the origin of the observer time, as this is when the first radiation is observed. We assign the pulse shape presented in § 2 beginning at this time to the overall observed signal.

We rearrange the shells after each collision as follows. Each shell moves from its earlier position $R_i(t_{j-1})$ to

$$R_i(t_j) \equiv R_i(t_{j-1}) + c\beta_i\,\delta t_j . \quad (14)$$

For the first collision, $t_{j-1} = 0$, and we use the "initial positions" here. All the shells except the $s$ shell and the $s + 1$ shell keep their Lorentz factor, the density, and the width: $\gamma_i$, $\rho_i$, and $l_i$. The $s$ and the $s + 1$ shell merge to form a single shell, which we label $s + 1$. We delete the $s$ shell, and from now on we will skip this index when it is encountered. Using the results of § 2, we now calculate the new parameters for the $s + 1$ shell: $\gamma_{s+1}$, $\rho_{s+1}$, and $l_{s+1}$.

We return now to the calculation of the distances between shells, $L_i$, and the corresponding collision times, $\delta t_i$. We find the next collision and proceed until there are no more collisions, i.e., until all the shells have merged to form a single shell or until the shells are ordered with increasing values of the Lorentz factor.

In order to reduce the number of parameters describing the wind, we adopt the following simplifications. We assume a constant initial width $l_i = l$ and constant initial separation $L_i = L$. In other words, we assume that the "inner engine" operates for a fixed period $l/c$ and then is quiet for a fixed period $L/c$.

We assume that the Lorentz factor of each shell is uniformly distributed between $\gamma_{\min}$ and $\gamma_{\max}$. For the distribution of the density we have two kinds of models. In the first kind we consider models in which the density, the mass, or the energy of each shell is a random variable which is uniformly distributed between 1 and some maximal value $X_{\max}$. In the second kind the density is correlated with the Lorentz factor as $\rho_i \propto \gamma_i^{\eta-1}$, so that the mass and kinetic energy of each shell are proportional to $\gamma_i^{\eta}$ and $\gamma_i^{\eta+1}$, respectively. For $\eta = 1$ the shells have equal density, for $\eta = 0$ the shells have equal mass, and for $\eta = -1$ the shells have equal energy. We will see later that the random density/mass/energy models give almost the same efficiency as the corresponding constant model, and the dependence on $X_{\max}$ is low. We therefore present most of the result for the correlation models, which are simpler.

Any timescale in this system is proportional to a sum of $L$ and $l$; the amplitudes of observed peaks depend neither on the absolute value of $l$ nor on that of $L$. If both of $L$ and $l$ are transformed by the same factor, we will get similar temporal profiles. We are interested in neither the absolute value of

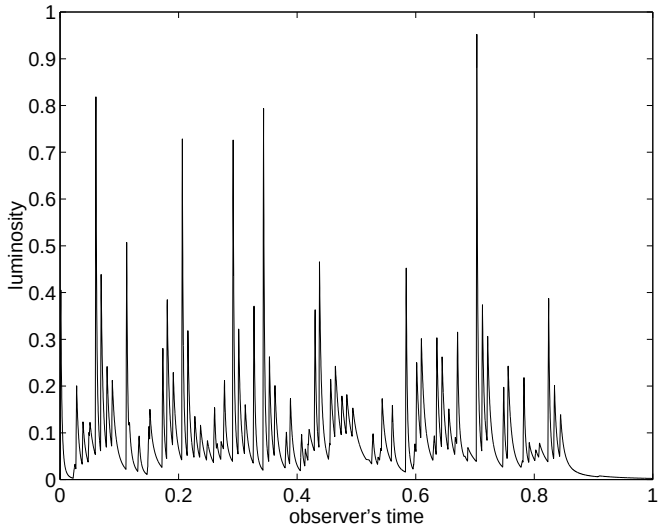


FIG. 2*a*

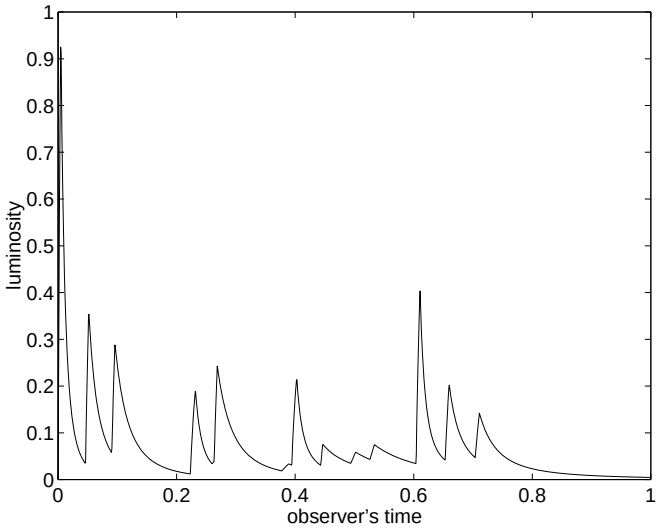


FIG. 2*b*

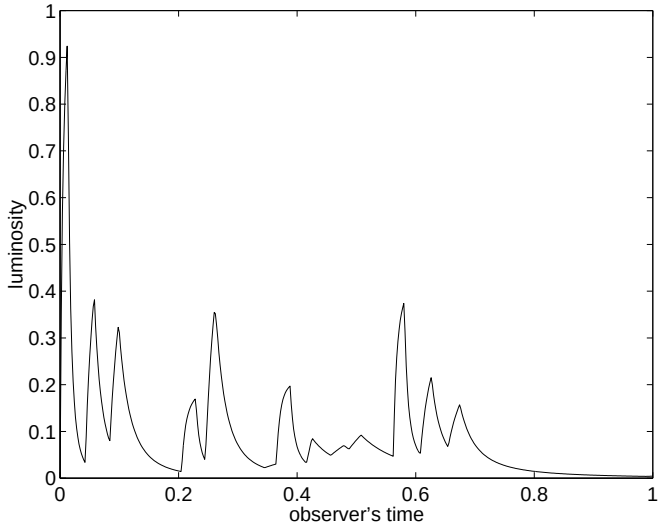


FIG. 2*c*

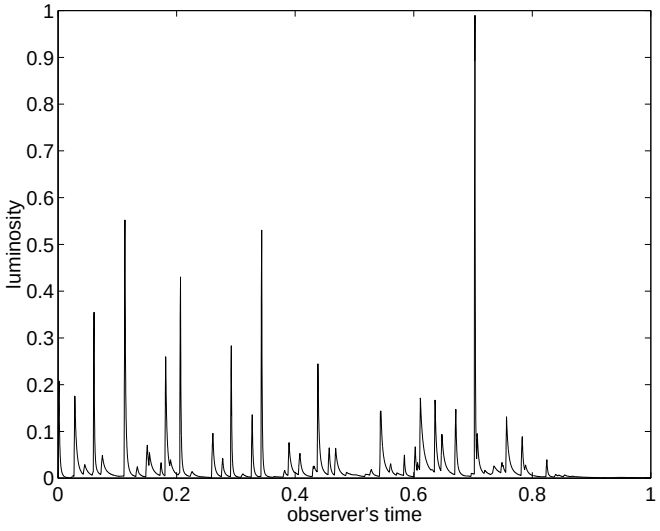


FIG. 2*d*

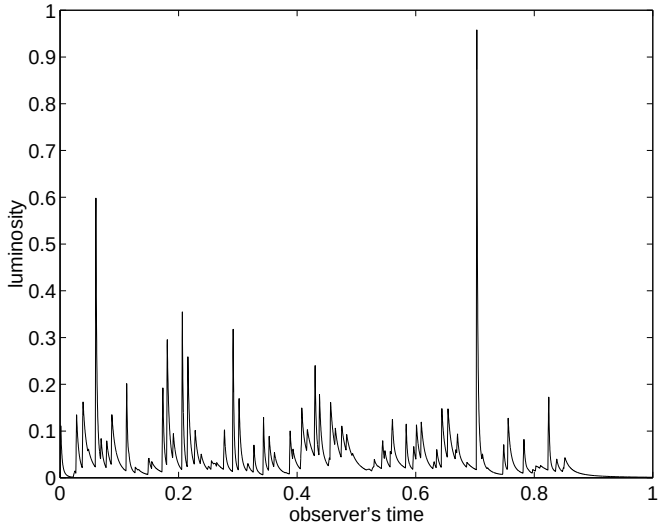


FIG. 2*e*

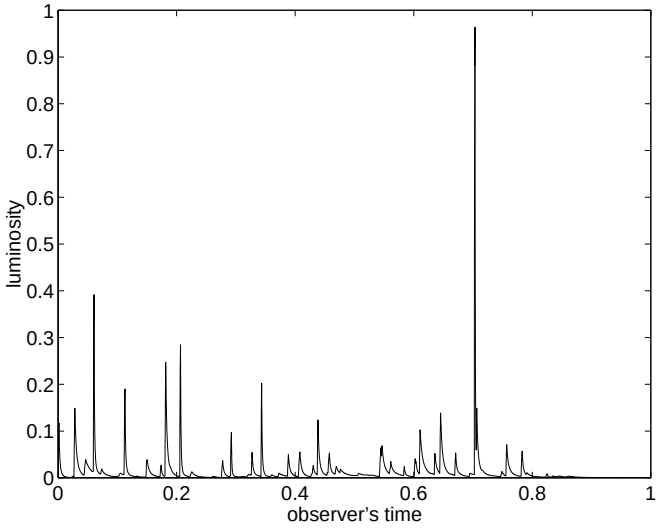


FIG. 2*f*

FIG. 2.—Observed temporal structures: Luminosity vs. observer's time, for different models. (*a*) $\gamma_{\min} = 100$, $\gamma_{\max} = 1000$, $N = 100$, $\eta = -1$, and $L/l = 5$. (*b*) $\gamma_{\min} = 100$, $\gamma_{\max} = 1000$, $N = 20$, $\eta = -1$, and $L/l = 5$. (*c*) $\gamma_{\min} = 100$, $\gamma_{\max} = 1000$, $N = 20$, $\eta = -1$, and $L/l = 1$. (*d*) $\gamma_{\min} = 100$, $\gamma_{\max} = 1000$, $N = 100$, $\eta = 1$, and $L/l = 5$. (*e*) $\gamma_{\min} = 100$, $\gamma_{\max} = 1000$, $N = 100$, random energy with $E_{\max} = 1000$, and $L/l = 5$. (*f*) $\gamma_{\min} = 100$, $\gamma_{\max} = 1000$, $N = 100$, random density with $\rho_{\max} = 1000$, and $L/l = 5$.

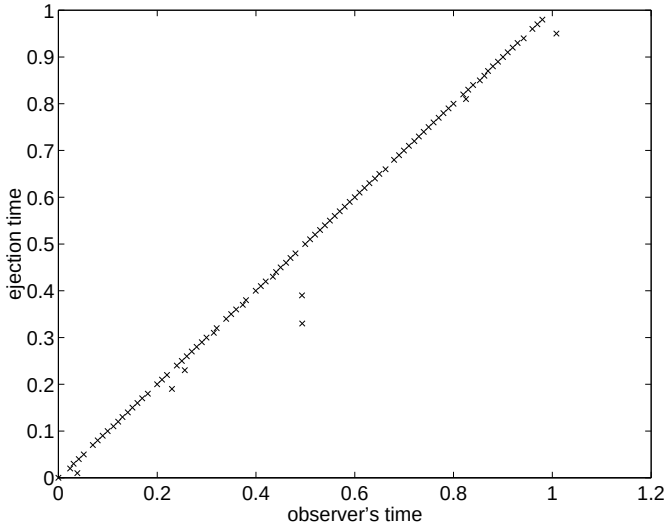


FIG. 3.—Time of ejection of a shell by the inner engine, $\tilde{t}_j$ vs. observed time of the photon produced in that shell, $t_{\mathrm{obs},j}$, for $N = 100$, $\gamma_{\min} = 10$, $\gamma_{\max} = 1000$, $\eta = -1$, and $L/l = 5$. The initial positions 0 and 100 correspond to the inner and outer edge of the wind.

the duration nor that of the peak; thus we can use a single parameter $L/l$ instead of the two parameters $L$ and $l$. The efficiency of the energy conversion by the shocks is independent of $L/l$. The total energy emitted is the sum of the energies emitted in the elementary two-shell collisions, which are independent of $L/l$. The density $\rho$ is the only quantity in this system with dimensions of mass. Therefore, only density ratio rather than density can determine the timescale, and the overall normalization of the density $\rho$ is also unimportant. Consequently, we find that there are only five initial parameters: $N$, $L/l$, $\gamma_{\max}$, $\gamma_{\min}$, and either $\eta$ (if the density is correlated with the Lorentz factor) or $X_{\max}$ (for random distribution of $\rho$, $m$, or $E$).

## 4. TEMPORAL STRUCTURE

The calculated temporal structure is a superposition of the pulses from the elementary two-shell collisions. Several typical temporal profiles are presented in Figures 2*a*–2*f*. Figure 2*a* depicts the luminosity for a model with $N = 100$ and $L/l = 5$ as a function of the observed time for shells with constant energy ($\eta = -1$). During the evolution of the $N$ shells, almost $N$ collisions happen and almost $N$ pulses are produced. Although some of the peaks are not observed because of their higher neighbors, the number of peaks is given by $\sim N$. In Figure 2*b* the luminosity is plotted with the same parameters as in Figure 2*a*, except that $N = 20$. Figures 2*a* and 2*b* show that $N$ practically determines the number of peaks. The width of a given peak $\delta T$ is determined by the emission timescale $\sim l/c$ or by the angular spreading $\sim L/c$. If the value of the separation $L$ is larger than that of the width $l$, $\delta T/T$ is $\sim 1/N$ and independent of $L/l$. In Figure 2*c* the luminosity is plotted with the same parameters as in Figure 2*b*, except that $L/l = 1$. The profile is almost independent of $L/l$.

The different amplitudes of the peaks originate mainly from the difference in $E_{\mathrm{int}}$, since all peaks have widths of the same order of magnitude, $\sim L/c$. For given random Lorentz factors, $E_{\mathrm{int}}$ depends on the index $\eta$ for models with density correlated to the Lorentz factor. The random Lorentz factors are uniformly distributed between $\gamma_{\min}$ and $\gamma_{\max}$. If $\gamma_{\max}/\gamma_{\min} \gg 1$, the ratio $\gamma_r/\gamma_s$ is typically large. In such a case, we obtain a simple formula,

$$E_{\mathrm{int}} \sim \begin{cases} (1 - 1/\sqrt{2})\gamma_r^2 & (\eta = 1)\,, \\ 2 - \sqrt{2} & (\eta = -1)\,. \end{cases} \tag{15}$$

For $\eta = -1$, $E_{\mathrm{int}}$ takes almost the same value for most of the collisions, so most of the peaks have comparable amplitudes (see Fig. 2*a*). Thus, for $\eta = -1$ we practically observe the "shell structure" produced by the inner source as almost all two-shell collisions produce an observable peak. If, on the other hand, $\eta = 1$ (see Fig. 2*d*), a few collisions produce significantly higher peaks than others and only those are observed. Thus the number of the observed peaks is much less than $N$, and the observed temporal structure corresponds only weakly to the activity of the inner source. Visual inspection suggests that the temporal structure produced by $\eta = -1$ better resembles the observed temporal structure.

Figures 2*e* and 2*f* present the luminosity profiles for models with random energy and random density, respectively. Both use $X_{\max} = 1000$, and both have a spread in the Lorentz factor $\gamma_{\max}/\gamma_{\min} = 10$. Again the random density is more spiky than the random energy case. However, as could be guessed intuitively, the random energy and the random density cases are more spiky than the constant-energy ($\eta = -1$; Fig. 2*a*) and constant-density ($\eta = 1$; Fig. 2*d*) cases, respectively.

The total width of the wind is $\Delta = Nl + (N - 1)L$. Neighboring shells collide on a timescale of $L\gamma^2/c$, with fluctuations of the same order of magnitude due to the fluctuations of $\gamma$. The matter is moving toward the observer; the resulting observed timescale is $L/c$. On the other hand, the difference in observed time due to the location of the given shell within the wind is of order $\Delta/c$. Since by definition $\Delta \gg L$, we observe pulses arising from collision between shells mostly according to their positions inside the wind, i.e., according to the time when those shells were emitted by the inner engine. In Figure 3 we plot the time when radiation is observed from a shell, $t_{\mathrm{obs},s}$, against the time when the shell was ejected from the source $\tilde{t}_s$. We associated the emission from a given collision with the slower shell. The clear correlation between the observed time and the time at which the source ejected the specific shell shows that the observed temporal structure reflects the activity of the source. This conclusion is valid even if there is a large spread in $\gamma$.

## 5. EFFICIENCY

We have shown that internal shocks could produce the highly variable temporal structure. We ask now what is the efficiency of this process? The relativistic shells collide with each other and merge into more massive shells. The overall efficiency of conversion of kinetic energy in internal shocks can be calculated from the initial and final kinetic energies as

$$\epsilon = 1 - \frac{\sum m_i^{(f)} \gamma_i^{(f)}}{\sum m_i^{(i)} \gamma_i^{(i)}}\,, \tag{16}$$

where the superscript $(f)$ and $(i)$ represent the initial and final values, respectively.

This efficiency depends on the model parameters $N$, $\gamma_{\min}$, $\gamma_{\max}$, and $\eta$ (or $X_{\max}$) and on the specific realization: the set of random Lorentz factors that are assigned to each shell.

TABLE 1

EFFICIENCIES WITH STANDARD DEVIATIONS FOR DIFFERENT MODELS

| $N$ | $\eta$ | $\gamma_{min}$ | $\gamma_{max}$ | Efficiency (%) |
|---|---|---|---|---|
| 100 ..... | 1 | 20 | 1000 | $10.9 \pm 1.4$ |
| 100 ..... | 1 | 50 | 1000 | $10.0 \pm 1.3$ |
| 100 ..... | 1 | 100 | 1000 | $8.5 \pm 1.1$ |
| 100 ..... | 1 | 200 | 1000 | $6.1 \pm 0.7$ |
| 100 ..... | 1 | 500 | 1000 | $1.7 \pm 0.2$ |
| 100 ..... | 0 | 20 | 1000 | $19.2 \pm 2.9$ |
| 100 ..... | 0 | 50 | 1000 | $16.0 \pm 2.3$ |
| 100 ..... | 0 | 100 | 1000 | $12.4 \pm 1.6$ |
| 100 ..... | 0 | 200 | 1000 | $7.7 \pm 0.9$ |
| 100 ..... | 0 | 500 | 1000 | $1.8 \pm 0.2$ |
| 100 ..... | −1 | 20 | 1000 | $25.0 \pm 3.5$ |
| 100 ..... | −1 | 50 | 1000 | $19.5 \pm 2.4$ |
| 100 ..... | −1 | 100 | 1000 | $14.1 \pm 1.6$ |
| 100 ..... | −1 | 200 | 1000 | $8.2 \pm 0.9$ |
| 100 ..... | −1 | 500 | 1000 | $1.8 \pm 0.2$ |
| 20 ..... | 1 | 100 | 1000 | $7.6 \pm 2.5$ |
| 20 ..... | −1 | 100 | 1000 | $11.0 \pm 3.3$ |
| 1000..... | 1 | 100 | 1000 | $8.7 \pm 0.3$ |
| 1000..... | −1 | 100 | 1000 | $15.1 \pm 0.5$ |
| 1000..... | −1 | 10 | 10000 | $39.3 \pm 2.6$ |

For each choice of the parameters of the model, we have evaluated the efficiency for 100 realizations. The mean efficiency and its standard deviation are listed in Tables 1 and 2.

The efficiency is only a few percent if the spread in the Lorentz factor is relatively low (a factor of 2–3). This agrees with the results of Mochkovitch et al. (1995), who concluded that the efficiency of this process is less than 10%. However, higher efficiency could be reached if the spread in $\gamma$ is larger. The spread required, for example, for 10% is $\gamma_{max}/\gamma_{min} \sim 6$ for $N = 100$ and $\eta = -1$.

TABLE 2

EFFICIENCIES WITH STANDARD DEVIATIONS FOR RANDOM PARAMETERS

| $N$ | Random Parameter | $\gamma_{min}$ | $\gamma_{max}$ | $X_{max}$ | Efficiency (%) |
|---|---|---|---|---|---|
| 100..... | $n$ | 100 | 1000 | 1000 | $8.2 \pm 1.2$ |
| 100..... | $m$ | 100 | 1000 | 1000 | $12.2 \pm 1.6$ |
| 100..... | $E$ | 100 | 1000 | 1000 | $14.2 \pm 1.6$ |

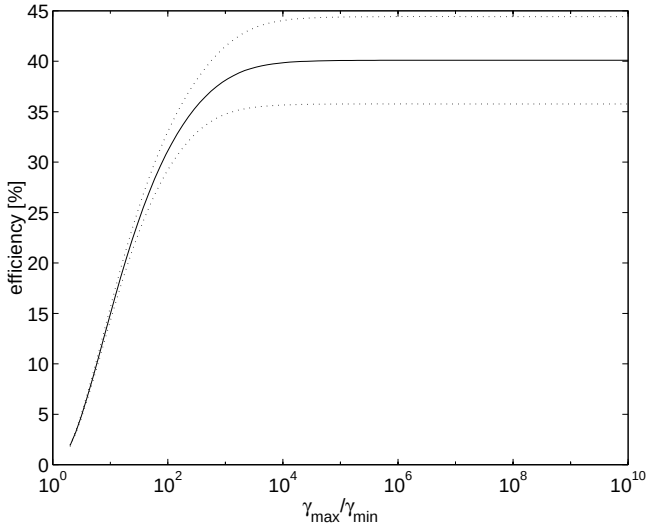


FIG. 4.—Efficiency vs. $\gamma_{max}/\gamma_{min}$ with 1 $\sigma$ error bars of 100 random simulations, for $\gamma_{min} = 10$, $N = 500$, and $\eta = -1$.

The efficiency is independent of $L/l$, which is important only for the temporal structure. For models with density correlated with the Lorentz factor the relevant parameters that determine the efficiency are $N$, $\eta$, $\gamma_{min}$, and $\gamma_{max}$ (see Table 1). For the random density models, we evaluated the efficiency with $X_{max} = 1$–1000. The efficiency is almost independent of $X_{max}$. It can be seen that the efficiencies of the models with random $n$, $m$, and $E$ are very similar to those with $\eta = 1$, 0, and −1, respectively (Table 2).

As the number of shells, $N$, increases, the kinetic energy of relative motion of the final mergers becomes negligible. The efficiency approaches an asymptotic value. Further, if we consider large values of $\gamma_{min}$, the efficiency depends only on

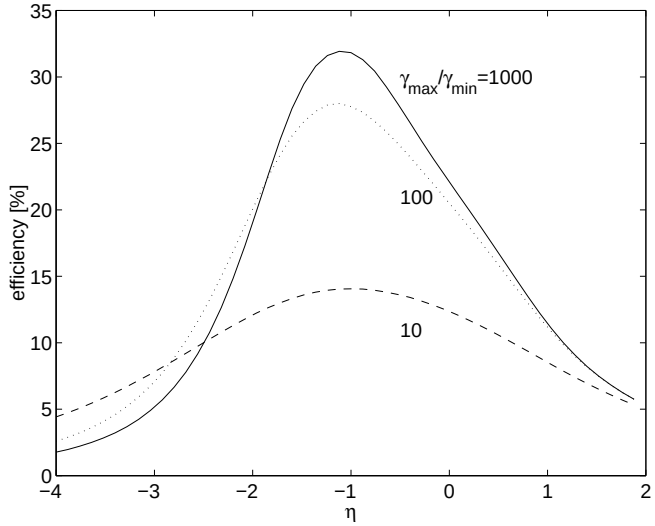


FIG. 5a

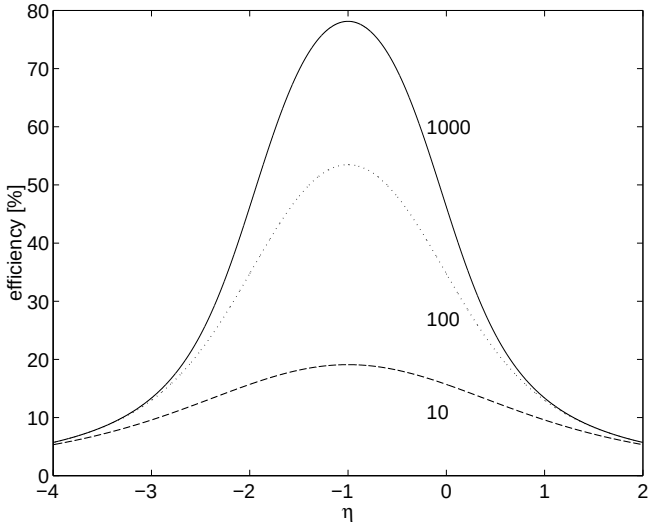


FIG. 5b

FIG. 5.—Efficiency vs. index $\eta$, for $\gamma_{min} = 100$, $N = 100$. The solid line corresponds to $\gamma_{max}/\gamma_{min} = 1000$, the dotted line to $\gamma_{max}/\gamma_{min} = 100$, and the dashed line to $\gamma_{max}/\gamma_{min} = 10$. (*a*) Numerical simulation. (*b*) Approximation by analytic formula (eq. [19]).

the ratio $\gamma_{\max}/\gamma_{\min}$ reaching an asymptotic value for large $\gamma_{\max}/\gamma_{\min}$ (Fig. 4). For models with correlation between the density and the Lorentz factor, this asymptotic value depends only on the index $\eta$. In the limits $\eta \to \pm\infty$, a single shell carries all the energy of the system and the energy and momenta of the other shells are negligible. Therefore, the massive shell is unaffected by collisions with the lighter ones. We expect a low efficiency in this limit (Fig. 5).

In order to understand the dependence of the efficiency on $\eta$, we consider a simplified model. Let all the shell collide and merge into a single shell and only then emit the thermal energy as radiation. Using conservation of energy and momentum, we can calculate the Lorentz factor and the efficiency:

$$\gamma = \sqrt{\sum \gamma_i^{\eta+1} / \sum \gamma_i^{\eta-1}}\,, \tag{17}$$

$$\epsilon = 1 - \sum \gamma_i^{\eta} / \sqrt{\sum \gamma_i^{\eta-1} \sum \gamma_i^{\eta+1}}\,. \tag{18}$$

Averaging over the random variables $\gamma_i$, and assuming a large number of shells $N \to \infty$, we obtain

$$\langle \epsilon \rangle \sim 1 - \frac{(\gamma_{\max}/\gamma_{\min})^{\eta+1} - 1}{\eta + 1} \times \sqrt{\frac{\eta(\eta+2)}{[(\gamma_{\max}/\gamma_{\min})^{\eta} - 1][(\gamma_{\max}/\gamma_{\min})^{\eta+2} - 1]}}\,. \tag{19}$$

This formula explains qualitatively the behavior of our numerical results. A comparison between the simulations in which the radiation is emitted right after each collision and the simplified single merge model is presented in Figure 5*b*.

An interesting point to notice is that for multishell collisions (both in the numerical simulation and in the simple model of eq. [19]) the most efficient case is where the shells have the same energy, while for the two-shell collision (eq. [3]) the highest efficiency is for shells with equal mass rather than equal energy.

## 6. CONCLUSIONS

Using a simple model, we have shown that internal shocks can produce the highly variable profile observed in most GRBs. There is a strong correlation between the time at which we observe a pulse and the emission time of the corresponding shell from the inner engine. This correlation persists even when there is a large spread in the Lorentz factor. Thus the observed temporal structure reproduces the activity of the source.

We have shown that the number of peaks is almost the same as the number of shells that the inner engine emitted. The separation between the peaks corresponds to the length of time during which the inner engine was quiet. The variability of peak heights can tell us whether all shells have comparable energy (low variability in observed peak heights) or not. A systematic statistical study comparing the temporal structure produced by internal shocks with observations will be carried out in a subsequent paper.

The efficiency of this process is low (less than 2%) if the initial spread in $\gamma$ is only a factor of 2. However, the efficiency could be much higher. The most efficient case is when the inner engine produces shells with comparable energies but with very different Lorentz factors. In this case ($\eta = -1$ and spread of the Lorentz factor $\gamma_{\max}/\gamma_{\min} > 10^3$) the efficiency is as high as 40%. For a moderate spread of the Lorentz factor $\gamma_{\max}/\gamma_{\min} = 10$, with $\eta = -1$, the efficiency is 20%.

We thank J. I. Katz for many useful discussion. S. K. gratefully acknowledges support by the Golda Meir Postdoctoral fellowship. This work was supported in part by a US-Israel BSF grant and by a NASA grant NAG 5-1904.

## REFERENCES

Fenimore, E. E., Madras, C. D., & Nayakshin, S. 1996, ApJ, 473, 998
Katz, J. I. 1994, ApJ, 432, L107
Meegan, C. A., et al. 1992, Nature, 355, 143
Mochkovitch, R., Maitia, V., & Marques, R. 1995, in Proc. 29th ESLAB Symp., Towards the Source of Gamma-Ray Bursts, ed. K. Bennett & C. Winkler (Noordwijk: ESTEC), 531
Narayan, R., Paczyński, B., & Piran, T. 1992, ApJ, 395, L83
Nemiroff, R. J., Noriss, J. P., Kouveliotou, C., Fishman, G. J., Meegan, C. A., & Paciesas, W. S. 1994, ApJ, 423, 432
Paczyński, B. 1990, ApJ, 363, 218
———. 1992, Nature, 355, 521
Piran, T. 1992, ApJ, 389, L45
———. 1996, in Unsolved Problems in Astrophysics, ed. J. Bahcall & J. P. Ostriker (Princeton: Princeton Univ. Press), 343
Rees, M. J., & Mészáros, P. 1994, ApJ, 430, L93
Sari, R., Narayan, R., & Piran, T. 1996, ApJ, 473, 204
Sari, R., & Piran, T. 1995, ApJ, 455, L143
———. 1997a, ApJ, in press
———. 1997b, MNRAS, in press
Shaviv, N., & Dar, A. 1995, MNRAS, 277, 287
Shemi, A., & Piran, T. 1990, ApJ, 365, L55